Photoelectron diffraction for probing valency and magnetism of 4f-based materials: A view on valence-fluctuating $EuIr_2Si_2$

D. Yu. Usachov,[1,*] A. V. Tarasov,[1] S. Schulz,[2] K. A. Bokai,[1] I. I. Tupitsyn,[1] G. Poelchen,[2,3] S. Seiro,[4] N. Caroca-Canales,[5] K. Kliemt,[6] M. Mende,[2] K. Kummer,[3] C. Krellner,[6] M. Muntwiler,[7] Hang Li,[8,7] C. Laubschat,[2] C. Geibel,[5] E. V. Chulkov,[1,9,10,11] S. I. Fujimori,[12] and D. V. Vyalikh[9,13]

[1]*St. Petersburg State University, 7/9 Universitetskaya nab., St. Petersburg, 199034, Russia*

[2]*Institut für Festkörper- und Materialphysik, Technische Universität Dresden, D-01062 Dresden, Germany*

[3]*European Synchrotron Radiation Facility, 71 Avenue des Martyrs, 38043 Grenoble, France*

[4]*Leibniz IFW Dresden, Helmholtzstr. 20, D-01069 Dresden, Germany*

[5]*Max Planck Institute for Chemical Physics of Solids, Nöthnitzer Str. 40, D-01187 Dresden, Germany*

[6]*Kristall- und Materiallabor, Physikalisches Institut, Goethe-Universität Frankfurt, Max-von-Laue Strasse 1, D-60438 Frankfurt am Main, Germany*

[7]*Paul Scherrer Institute, Swiss Light Source, CH-5232 Villigen, PSI, Switzerland*

[8]*Department of Energy Conversion and Storage, Technical University of Denmark, Anker Engelunds Vej 411, DK-2800 Kgs. Lyngby, Denmark*

[9]*Donostia International Physics Center (DIPC), 20018 Donostia/San Sebastián, Basque Country, Spain*

[10]*Departamento de Física de Materiales UPV/EHU, Centro de Física de Materiales CFM MPC and Centro Mixto CSIC-UPV/EHU, 20080 San Sebastián/Donostia, Spain*

[11]*Tomsk State University, Lenina Av. 36, 634050, Tomsk, Russia*

[12]*Materials Sciences Research Center, Japan Atomic Energy Agency, Sayo, Hyogo, 679-5148, Japan*

[13]*IKERBASQUE, Basque Foundation for Science, 48013, Bilbao, Spain*

(Received 27 July 2020; revised 2 October 2020; accepted 12 October 2020; published 2 November 2020)

We present and discuss the methodology for modeling 4f photoemission spectra, 4f photoelectron diffraction (PED) patterns, and magnetic dichroism effects for rare-earth-based materials. Using PED and magnetic dichroism in photoemission, we explore the electronic and magnetic properties of the near-surface region of the valence-fluctuating material $EuIr_2Si_2$. For the Eu-terminated surface, we found that the topmost Eu layer is divalent and exhibits a ferromagnetic order below 10 K. The valency of the next Eu layer, that is the fifth atomic layer, is about 2.8 at low temperature that is close to the valency in the bulk. The properties of the Si-terminated surface are drastically different. The first subsurface Eu layer (fourth atomic layer below the surface) behaves divalently and orders ferromagnetically below 48 K. Experimental data indicate, however, that there is an admixture of trivalent Eu in this layer, resulting in its valency of about 2.1. The next deeper lying Eu layer (eighth atomic layer below the surface) behaves mixed valently, but the estimated valency of 2.4 is notably lower than the value in the bulk. The presented approach and obtained results create a background for further studies of exotic surface properties of 4f-based materials, and allow us to derive information related to valency and magnetism of individual rare-earth layers in a rather extended area near the surface.

DOI: 10.1103/PhysRevB.102.205102

I. INTRODUCTION

Photoelectron diffraction (PED) is well established as an efficient method for detailed structural analysis of crystalline surfaces, defects and impurities, thin films, adsorbates, two-dimensional (2D) materials, and other systems [1–7]. It is based on the fact that photoelectrons emitted from the atomic sites, called emitters, experience multiple scattering on the surrounding atoms when they propagate to the sample surface. As a result, the angular distribution of the measured photocurrent represents a diffraction pattern, which contains information about the local environment of the emitters. In a common PED experiment, electrons are emitted from the closed core shell, leaving the atom with a core hole. Interactions of the core hole with valence electrons may give rise to several spectral components, known as the atomic multiplet. The photoemission (PE) intensities of the multiplet components are sensitive to the local magnetic order in the system even in the absence of net magnetization [8], enabling PED-based insight into magnetic phase transitions in the near-surface region.

In the case of nonradiative decay of the core hole, Auger electrons are produced, giving rise to a so-called Auger electron diffraction [9]. Both direct PE and Auger processes can be combined to selectively increase the signal from the atoms of interest by an order of magnitude or even more. This is realized in resonant PED experiments, when the photon energy is selected close to the absorption edge of a core shell [6,10,11], being particularly useful for studies of impurities and defects at low concentrations [11].

*dmitry.usachov@spbu.ru

While PED became a routine technique when based on PE from a closed shell, it may also be of interest to consider emission from an open shell. This is of particular importance for studies of materials containing rare-earth elements. Their open $4f$ shells are sufficiently localized to be treated as core states. However, the capabilities of PED analysis based on $4f$ multiplets of lanthanides remain rather unexplored.

Here, we developed a methodology of PED experiments with the aim to study the properties of $4f$ materials. We consider the case of a layered Eu-based system, namely, the valence-fluctuating material $EuIr_2Si_2$ [12,13], and explore to which extent we can use PED for characterization of such properties as valency and magnetic order at the surface and deeper atomic layers.

Discovered in 1986, $EuIr_2Si_2$ has recently reappeared as a focus of research interest due to its explicit ferromagnetic properties at the Si-terminated surface, where both spin-orbit coupling and exchange magnetic interaction are involved [14]. The layered structure of this compound is composed of Si-Ir-Si trilayer blocks which separate valence-fluctuating Eu layers. The well-established bulk properties show a nonmagnetic behavior of the Eu layers, while its valency changes strongly with temperature, ranging from a value of 2.8 at rather low temperatures to 2.3 at room temperature [12,15,16].

Due to their structural and bonding characteristics, single crystalline samples of this compound can cleave between Eu and adjacent Si layers, resulting in either Eu- or Si-terminated surfaces. For the Si-terminated crystal, the Eu ions in the subsurface layer, i.e., the fourth atomic layer below the Si-Ir-Si surface block, surprisingly reveal not only a divalent behavior, but also a long-range ferromagnetic order of $4f$ magnetic moments below 48 K [14]. As a result, the appearance and peculiar interplay of the exchange field from the Eu $4f$ magnetic moments and the spin-orbit field originating from the Ir atoms leads to an unusual spin structure of the 2D electron states on the Si-terminated surface [14,17].

So far, only the subsurface Eu layer of the Si-terminated surface has been studied and discussed in detail. While this made it possible to describe the magnetic properties of the Si-terminated surface in a general way, several essential open questions remain that need to be comprehensively addressed: (i) What can be said regarding the next deeper Eu in the eighth atomic layer below the Si-terminated surface? Does it already reveal a noninteger valence state as found in the bulk? (ii) What are the properties of the surface and subsurface Eu for the Eu-terminated surface? It is quite probable that the Eu surface of $EuIr_2Si_2$ behaves divalently, like in all known noninteger-valent or trivalent Eu systems, where the surface valence transition is caused by the reduced coordination at the surface and a related shift of the $4f$ states to higher binding energies. But does the Eu surface layer also order magnetically, and what happens to the valency and magnetic order in the subsurface of an Eu-terminated crystal?

In the present paper, we show that classical PED can be a useful method to address these questions and allows us to discuss both the valency and magnetism of Eu in the surface and subsurface regions. Generally and qualitatively, the valence-fluctuating state of matter can be easily established in photoelectron spectroscopy measurements. For Eu-based systems, it is manifested by the appearance of $4f^5$ and $4f^6$ final-state multiplets. They result from direct photoionization of the trivalent $4f^6$ and divalent $4f^7$ configurations of the Eu atoms, respectively. The mean valency can be determined to a certain extent from the intensity ratio of these two final-state multiplets. However, the derived value will be obtained under a set of assumptions, particularly regarding the photoionization cross sections, the valency of individual layers and the subsurface core-hole effect [18]. We show that with the help of PED one can determine separately the contributions from individual Eu layers to the respective diffraction patterns of both the divalent and trivalent emissions and thus derive the values of Eu valency in different layers. In addition, we simultaneously obtain information about possible relaxation or reconstruction phenomena near the surface. Finally, the obtained PED data have allowed us to make conclusive statements on the magnetic order of Eu layers in the near-surface region.

II. METHODS

High-quality single-crystalline samples of $EuIr_2Si_2$ were cleaved *in situ* under ultrahigh vacuum conditions at a temperature of 35 K. The obtained surface exhibited large (hundreds of microns in size) terraces with either Eu or Si termination, which were easily identified by x-ray photoelectron spectroscopy (XPS).

PED measurements were performed at the X03-DA (PEARL) beamline [19] of the Swiss Light Source (SLS). The normal to the sample surface, the x-ray beam, the polarization vector of photons, and the axis of the analyzer lens were oriented in the horizontal plane, while the entrance slit of the Scienta EW4000 electron analyzer was oriented vertically. PED maps were measured by rotating the sample with a polar angle step of 1° and an azimuthal angle step of 15°, while the acceptance angle of the analyzer was about $\pm 25^\circ$. The 2D electron detector allowed mapping of the angular distribution with an azimuthal angle step of less than 0.5°. The data were obtained at a temperature of about 30 K using linearly polarized radiation with the photon energies of 141 eV for Eu^{2+} and 145 eV for Eu^{3+} ions. The $4f$ core-level PE measurements at a temperature of 1 K were carried out at the UE112-PGM-2b-1^3 beamline of the BESSY II synchrotron (Helmholtz Zentrum Berlin). Temperature dependence of Eu $4f$ spectra was measured at the SIS-ULTRA station of the SLS. Calculations of PED patterns and one-electron PE matrix elements were performed using the EDAC code [20]. In these calculations, we used a geometry with rotating sample and fixed emission direction, thus, simulating the measurement process. Uncertainties were estimated in accordance with Ref. [21].

III. RESULTS AND DISCUSSION

A. Structure and XPS characterization

Due to its layered structure, $EuIr_2Si_2$ single crystals cleave between the Eu and Si atomic layers, resulting in two possible surface terminations with the near-surface region of both terminations shown schematically in Fig. 1. For the Si-terminated surface presented in the upper part, the two Eu layers closest to the surface are from hereon referred to as fourth and eighth Eu layers, respectively. For the Eu-terminated surface shown in the lower part, the surface Eu

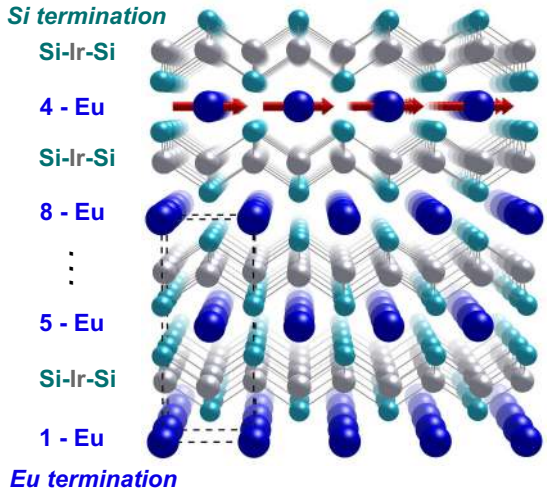

FIG. 1. Structure of the $EuIr_2Si_2$ crystal and surfaces. Dashed lines show the tetragonal unit cell. Arrows indicate magnetic moments of Eu^{2+} ions in the fourth atomic layer of the Si-terminated surface.

layer as well as the next subsurface Eu layer are referred to as first and fifth Eu layers. The freshly cleaved surface of $EuIr_2Si_2$ usually reveals a mosaic pattern of Si- and Eu-terminated terraces, which can be readily distinguished in PE measurements due to their remarkably different features in the $4f$-sensitive PE spectra.

In PED experiments, the first and essential question is which photon energy is better to be used for acquisition of the PED patterns. The difficulties in our case are linked to the strong valence-band emission, which stems mainly from Ir $5d$ states overlapping with the Eu $4f$ final state multiplet. To increase the $4f$ signal, we decided to use the photon energy, which corresponds to the Fano resonance at the Eu $4d \rightarrow 4f$ threshold. This allows us to considerably enhance the emission from Eu $4f$ states in comparison to the valence-band emission. We have checked the PE intensities of the Eu $4f$ multiplets across the resonance and found the appropriate photon energies to be ∼141 eV and ∼145 eV. They correspond to the maximal cross sections of the Eu $4f$ emission for the Eu^{2+} and Eu^{3+} configurations, respectively [14,22]. It is worth noting that, in general, the spectral pattern of the multiplet may change when passing the resonance. This point will be discussed further in more detail.

Figure 2(a) shows the $4f$ core-level PE spectrum taken from a freshly cleaved Si-terminated surface of $EuIr_2Si_2$. The Eu^{3+} $4f$ signal is represented mainly by the set of ^6H, ^6F, and ^6P components. The Eu^{2+} $4f$ final-state multiplet is located in the low-binding-energy region that is shown in Fig. 2(b) in detail. Its individual $^7F_{J'}$ terms, where $J' = 0...6$, are well resolved. This $4f$ spectral pattern is usually associated with the "bulk" Eu $4f$ emission [23], although it still reflects the properties of the near-surface region due to the small escape depth of photoelectrons. In our case, it is reasonable to suppose that mainly the fourth and to some extent the eighth Eu layers contribute to the measured $4f$ PE signal. The extended side peak, seen at the binding energy of 1.6 eV, is related to the emission from the Ir $5d$ valence band as well as from residual Eu^{2+} ions, which may be present on the surface.

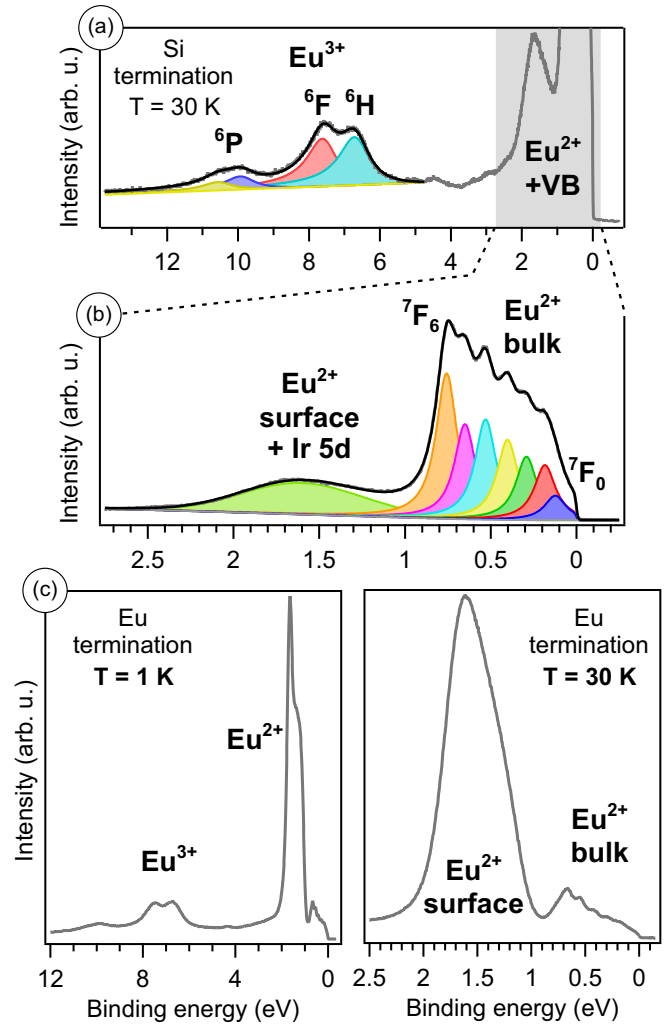

FIG. 2. PE spectra taken from Si- (a), (b) and Eu- (c) terminated surfaces of $EuIr_2Si_2$. The spectra were measured at the $4d \rightarrow 4f$ Fano resonance of Eu^{3+} at the photon energy of 145 eV.

The $4f$ core-level PE spectra from an Eu-terminated surface are shown in Fig. 2(c). It is rather different to that obtained from a Si-terminated surface. It consists of an Eu^{2+}-bulk emission near the Fermi level, which is relatively weak, similarly to the Eu^{3+} emission, and a huge Eu^{2+} surface component shifted with respect to the Eu^{2+}-bulk component by a surface energy shift of about 1 eV to higher binding energies. From the large binding energy of the surface component, one may conclude that the surface layer is fully divalent [23]. Since its underlying multiplet structure is much less resolved than in case of the bulk component, we will consider only the angular distribution of its total intensity for the following analysis.

Before turning to the investigation of the experimentally derived PED data from both Si- and Eu-terminated surfaces of $EuIr_2Si_2$, we would like to present and discuss the underlying theoretical model. It will help us get information on the structural properties of each surface as well as on the magnetic properties and valency of Eu in each individual layer. Please note that some assumptions had to be made, which might lead to the impression that the model is rather oversimplified. But,

as we will demonstrate further, the PED data computed on its basis agree well with our experimental results and allow us to make conclusive statements on the properties of Eu layers for both considered surface terminations.

B. Photoemission from the 4*f* shell of Eu

To model the spectral features of PE from the open $4f$ shell of Eu atoms and to compute PED patterns, we used the following approximations. We neglect the crystal-electric-field (CEF) splitting of electronic states in both initial and final states. The initial state of Eu^{2+} is characterized by zero orbital momentum ($L = 0$), while the initial state of Eu^{3+} has zero total momentum ($J = 0$), hence, CEF effect is negligible in both cases. For the final states, CEF splitting may be noticeable, but it is expected to be smaller than the half-width of PE peaks, which is about 90 meV for Eu^{2+} multiplet components due to lifetime broadening and energy resolution; therefore, it can also be neglected. Further, we use an open-core approximation where $4f$ electrons act as core states without hybridization with valence states. Consequently, we ignore any additional spectral structures in the momentum-resolved $4f$-emission patterns linked to avoided-crossing gaps [24,25], which are of minor importance in our case. We work in the Russell-Saunders limit of weak spin-orbit coupling and treat the PE process nonrelativistically.

In spite of carrying out measurements at the $4d \rightarrow 4f$ resonance, we consider only the direct photoexcitation channel and ignore the possible influence of the Auger decay channel on the angular distribution of photoelectrons. The latter assumption can be justified by the fact that the observed final state spectral features are equivalent to those that would result from a direct PE process [26,27]. For Eu^{2+} ions, we have checked that the spectral shape of their relatively narrow $4f$ multiplet at the resonance maximum is similar to the off-resonance case that was also observed in the previous studies of Tb [28]. For Eu^{3+} ions, the relative intensities of the multiplet components are notably different in the resonant and nonresonant emissions, probably because the multiplet components are spread over a wider energy range. However, this is not crucial for the analysis of Eu^{3+} PED data, in which the absolute intensities were ignored and only the angular dependencies were analyzed. Note that the angular dependence of the photocurrent at the resonance may differ from the off-resonant case. However, it was shown that the angular asymmetry parameter of the Eu $4f$ differential cross section exhibits significant deviations from its value for direct PE only at photon energies lower than the energy of the cross section maximum [22]. In our calculations, we have checked that possible changes of the PE matrix elements and phases of d and g partial waves at the resonance maximum lead to negligible changes of the resulting PED patterns. As we will show further on, the computed $4f$ PED patterns on the basis of the above-listed approximations demonstrate quite good agreement with those derived experimentally, giving valuable insight into the properties of Eu layers near the surface for both terminations.

In the light of these approximations, the differential cross section of transition from the initial state $|wLSJM_J\rangle$ to the final states $|w'L'S'J'M'_J\rangle$ with all possible M'_J may be written as [29]

$$\sigma_{M_JJ'}(\vec{e}) = NQ^2(wLS|w'L'S') \times \sum_{mm_sM'_J} U^2(LSJM_J|L'S'J'M'_Jlmm_s)\sigma_m(\vec{e}), \quad (1)$$

where w is a set of quantum numbers, which distinguishes different states with identical quantum numbers LSJ, while N is the occupation number of the $4f$ shell. The factor $Q(wLS|w'L'S')$ is the fractional parentage coefficient and $\sigma_m(\vec{e})$ is the one-electron differential PE cross section of the $4f$ orbital lm. The vector $\vec{e}$ indicates the PE direction defined by azimuthal and polar angles and U represents the following recoupling coefficients [29], involving four Clebsch-Gordan coefficients:

$$U(LSJM_J|L'S'J'M'_Jlmm_s) = \sum_{\substack{MM_S \\ M'M'_S}} C^{LM}_{L'M'\,lm} C^{SM_S}_{S'M'_S\,\frac{1}{2}m_s} C^{JM_J}_{LM\,SM_S} C^{J'M'_J}_{L'M'\,S'M'_S}. \quad (2)$$

By means of standard algebraic manipulations [30], we obtain

$$U^2 = (2L+1)(2S+1)\left[\sum_{k\varkappa}(2k+1)C^{JM_J}_{\frac{1}{2}m_s\,k\varkappa} C^{J'-M'_J}_{lm\,k-\varkappa} \times \begin{Bmatrix} L & S & J \\ \frac{1}{2} & k & S' \end{Bmatrix}\begin{Bmatrix} L & L' & l \\ J' & k & S' \end{Bmatrix}\right]^2. \quad (3)$$

For the case of Eu^{2+} ions, the $4f$ shell is half filled ($N = 7$), the initial state term is $^8S_{7/2}$, and the final state term is $^7F_{J'}$. In this case, $Q = 1$ and $L = 0$. Hence, the Wigner 6-j symbols in Eq. (3) vanish and we obtain

$$\sigma^{Eu^{2+}}_{M_JJ'}(\vec{e}) = \sum_{mm_s\ M'_SM'_J}\left(C^{JM_J}_{\frac{1}{2}m_s\,S'M'_S} C^{J'M'_J}_{lm\,S'-M'_S}\right)^2\sigma_m(\vec{e}). \quad (4)$$

In the case of zero temperature, when only the lowest magnetic sublevel $M_J = -J$ is occupied, we get

$$\sigma^{Eu^{2+}}_{J',M_J=-J}(\vec{e}) = \sum_m \left(C^{J'(3+m)}_{3m\,33}\right)^2\sigma_m(\vec{e}). \quad (5)$$

Since all $\sigma_m(\vec{e})$ are different, it is obvious from Eq. (5) that the angular distributions of the PE intensity will be different for spectral peaks with different J'. This conclusion will be directly confirmed experimentally.

Let us consider the one-electron cross section, which is given by

$$\sigma_m(\vec{e}) \propto |\langle f \mid \vec{\varepsilon}\cdot\vec{r} \mid lm\rangle|^2, \quad (6)$$

where $|f\rangle$ is the continuum final state of the photoelectron and $\vec{\varepsilon}$ is the photon polarization vector. The quantum number m describes the orbital momentum projection on the magnetization direction. Thus, the cross section depends on the photon polarization and magnetization direction.

In calculations of angular dependencies of one-electron PE matrix elements for atoms in the crystal lattice, PED must be taken into account. For this purpose, we use the EDAC code [20], which is widely applied to calculate PED at the crystal surface. To include magnetization dependence of the matrix elements, we perform rotation of the quantization axis,

which is initially fixed along the surface normal in the EDAC program. To rotate the quantization axis to the direction of magnetization, we use the complex conjugate of the Wigner D-matrix $D^*(\alpha, \beta, \gamma)$:

$$\langle f \mid \vec{\varepsilon} \cdot \vec{r} \mid lm \rangle = \sum_{m'} D^{l\,*}_{mm'}(\alpha, \beta, \gamma) \langle f \mid \vec{\varepsilon} \cdot \vec{r} \mid lm' \rangle , \quad (7)$$

where (α, β, γ) is a set of Euler angles, which define the magnetization direction relative to the surface normal. The matrix elements in the right part of Eq. (7) are directly calculated with the EDAC program.

Equation (5) already allows us to obtain rather good agreement with experimental data. However, it can be further improved by taking into account the temperature-dependent occupation of the magnetic sublevels M_J. According to the Weiss molecular-field theory [31], the occupation is given by

$$u_{M_J} = \frac{\sinh\left(\frac{y}{2J}\right)}{\sinh\left(\frac{2J+1}{2J}y\right)} \exp\left(-y\frac{M_J}{J}\right), \quad (8)$$

where y is a solution of the equation

$$B_J(y) = y\frac{(J+1)T}{3JT_C} .$$

Here, $B_J(y)$ is the Brillouin function

$$B_J(y) = \frac{2J+1}{2J}\coth\left(\frac{2J+1}{2J}y\right) - \frac{1}{2J}\coth\left(\frac{y}{2J}\right),$$

T is the sample temperature (30 K in our experiment), and T_C is the Curie temperature. As we know [14], the Si-terminated surface of $EuIr_2Si_2$ reveals ferromagnetic properties below $T_C = 48$ K. The temperature-dependent cross section is given by summation over all M_J:

$$\sigma_{J'}(\vec{e}) = \sum_{M_J} u_{M_J} \sigma_{M_J J'}(\vec{e}). \quad (9)$$

In the case of nonmagnetic Eu^{3+} ions or in the paramagnetic (PM) state of divalent Eu, all occupation numbers are $u = (2J+1)^{-1}$ and Eq. (9) leads to

$$\sigma_{J'}(\vec{e}) = \sigma_a(\vec{e}) Q^2(wLS|w'S'L')(2J'+1)(2L+1)(2S+1) \times N \sum_{k=J\pm\frac{1}{2}} (2k+1) \begin{Bmatrix} L & S & J \\ \frac{1}{2} & k & S' \end{Bmatrix}^2 \begin{Bmatrix} L & L' & l \\ J' & k & S' \end{Bmatrix}^2 , \quad (10)$$

where $\sigma_a(\vec{e}) = (2l+1)^{-1}\sum_m \sigma_m(\vec{e})$ is the average one-electron cross section. However, in our PED analysis, the whole Eq. (10) is not needed. We only use the fact that $\sigma_{J'}(\vec{e}) \propto \sigma_a(\vec{e})$. In other words, the angular dependencies of intensities of all multiplet components are identical for the nonmagnetic case and follow the angular dependence of a closed shell. They only differ by a coefficient.

C. Photoelectron diffraction analysis

Having established the model for calculations of Eu $4f$ PED patterns, let us turn to the comparative analysis of the computed and experimentally derived PED data for Si- and Eu-terminated surfaces which are shown in Fig. 3. They represent the measured angular distributions of the PE intensity after subtraction of a smooth background I_0 in accordance with Ref. [21]. The measured and calculated patterns of the Eu^{2+} signal were obtained by intensity integration over all seven J' components. In this case, the total cross section, given by summation of Eq. (4) over J', is simply $\sigma(\vec{e}) = 7\sigma_a(\vec{e})$. We have found that all measured patterns reveal the fourfold symmetry of the lattice, therefore, in Fig. 3 we show the intensities, which were additionally symmetrized to reduce noise and minimize possible influence of deviations of the emission direction from the horizontal plane. In the case of Eu^{3+}, we only analyzed the PED pattern of the ^6F peak because it overlaps less with the valence states than the ^6H line.

Let us turn now to the PED analysis of the Si-terminated surface. Since the thickness of the four-layer Si-Ir-Si-Eu block is only 5 Å and we expected the inelastic mean-free path to have a similar length, the relative normal-emission intensities from the Eu atomic layers may exponentially decay with depth as 1, 0.37, and 0.14 for the fourth, eighth, and 12th layers, respectively. Therefore, in our PED modeling we considered the PE from the Eu fourth, eighth, and 12th atomic layers. We assumed that each layer contains both Eu^{2+} and Eu^{3+} ions with an unknown ratio of their concentrations. The concentrations were fitted together with the inner potential and inelastic mean-free path to reach the minimum of the reliability factor (R factor [21]) for the two PED patterns [Figs. 3(a) and 3(b)] simultaneously. It should be noted that in our analysis the absolute intensities of the Eu PE lines were not used, since their cross sections near the resonance are not well known. Only relative intensity variations as a function of emission angles were analyzed. The resulting calculated PED patterns are shown in Figs. 3(f) and 3(g). They both exhibit a R factor of 0.21, which is qualified as a good agreement. The R-factor analysis shows a valency of 2.15 ± 0.15 for the fourth Eu layer, while for the valency of the eighth Eu layer we obtained the value of 2.55 ± 0.4. Further, we will show that additional PE measurements of Eu^{2+}/Eu^{3+} intensities performed at several photon energies allow us to reduce these uncertainties. The 12th Eu layer valency cannot be determined due to its small contribution to the PED pattern. We determined the inner potential as $V_0 = 13.2 \pm 1.3$ eV for the Si-terminated surface and 12.3 ± 1.3 eV for the Eu termination.

First, we should say that the obtained results are consistent with our previous studies [14,17], where the density-functional theory (DFT) calculations have demonstrated good agreement with the measured valence band dispersions under the assumption that Eu in the fourth layer is fully divalent, while the eighth and deeper layers have noninteger occupation of the $4f$ shell, which corresponds to a mean valency of 2.8. The next essential point is that the estimated uncertainties are rather large. The reason for this is a strong correlation between the valencies in the fourth and eighth layers as the parameters of our model. For example, if the Eu^{3+} concentrations in the fourth and eighth layers are decreased by a factor of 2, the Eu^{3+} pattern will remain unchanged, while the Eu^{2+} pattern will exhibit only minor changes, because the divalent Eu signal originates predominantly from the fourth layer and because the PED patterns from the fourth and eighth layers exhibit many similar features [see Figs. 3(k) and 3(l)]. As a result, our PED analysis is not able to quantify concentrations precisely. However, our analysis clearly indicates that

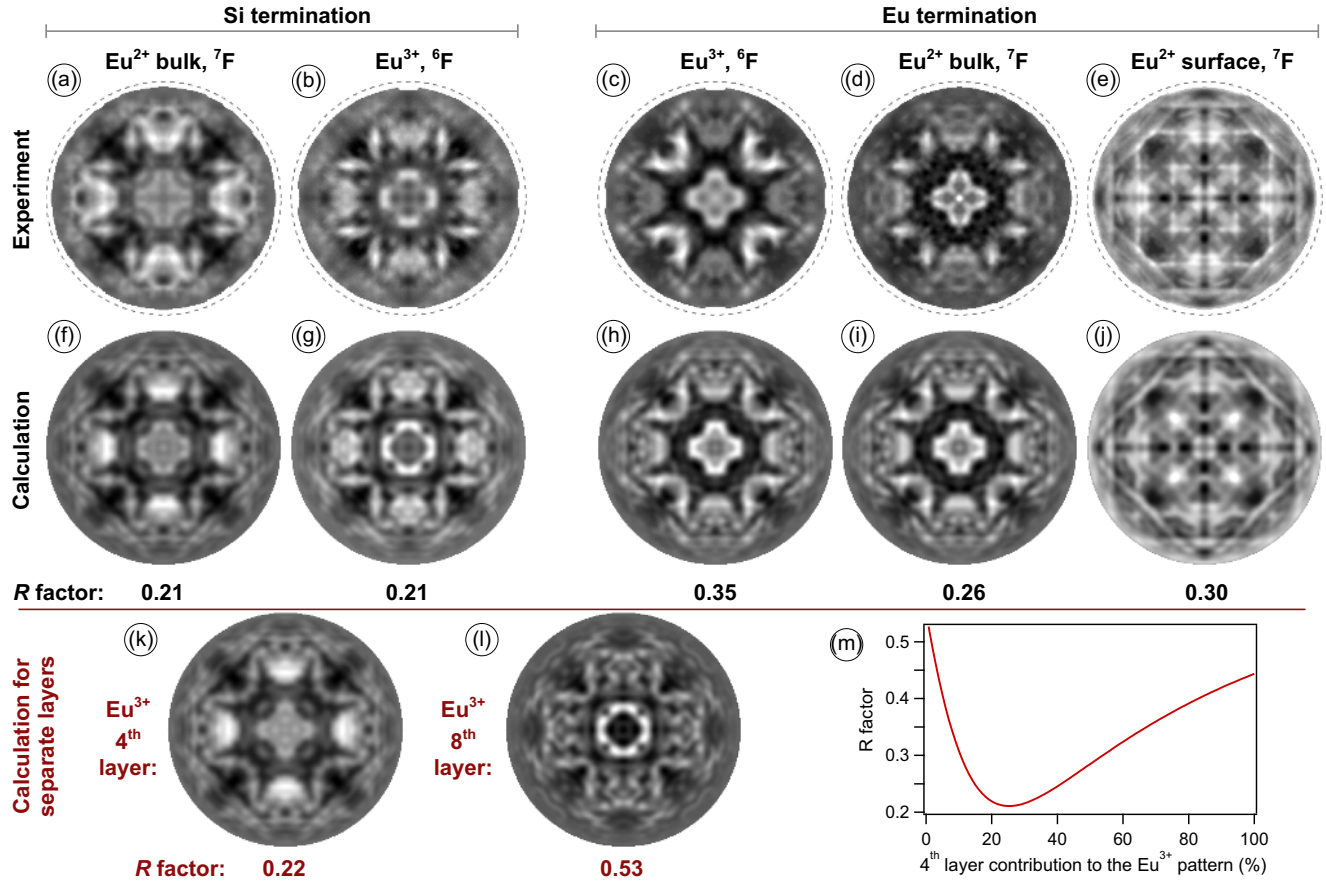

FIG. 3. (a)–(e) Experimental and (f)–(j) computed PED patterns of the $EuIr_2Si_2$ surfaces. The data are presented in orthographic projection with subtracted background intensity. Dashed circles correspond to the polar emission angle of 90°. Computed patterns represent the average one-electron cross section σ_a. (k), (l) Theoretical PED patterns for Eu^{3+} ions in the fourth and eighth Eu layers of the Si-terminated surface. (m) *R* factor for the experimental PED pattern (b) and a mixture of theoretical patterns (k) and (l) as a function of relative contribution of the pattern (k).

the valency in the fourth layer is higher than 2.0. This is illustrated in Fig. 3(m), which shows the *R* factor of the Eu^{3+} pattern as a function of mixing ratio of the two PED patterns calculated for the fourth and eighth layers [Figs. 3(k) and 3(l)]. The pronounced minimum in the *R*-factor curve indicates that the ratio of Eu^{3+} concentrations in the eighth/fourth layers is about 3.5 ± 1.5.

Let us turn to the Eu-terminated surface of $EuIr_2Si_2$. Already from the brief overview of the $4f$ core-level PE data in Fig. 2(c), it is clear that the topmost Eu layer exhibits an explicitly divalent state [23,32]. The measured and computed PED patterns for the Eu- surface are shown in Figs. 3(e) and 3(j), respectively. Good agreement between theory and experiment indicates that after cleavage the sample surface remains unreconstructed. The *R*-factor analysis of the PED data allowed us to determine the Eu-Si interlayer distance, which was found to be 1.22 ± 0.03 Å. It is worth noting that our DFT calculations based on the local density approximation to exchange-correlation potential [14] predicted an inward relaxation of the topmost Eu layer, which results in the spacing of 1.22 Å at the surface, while it is 1.27 Å in the bulk. Thus, the value of the interlayer distance obtained from the PED analysis matches perfectly the value obtained with DFT.

Now, if we compare the PED patterns taken from Eu^{3+} [Fig. 3(c)] and Eu^{2+} [Fig. 3(d)], where the latter is the so-called bulk component of the Eu $4f$ spectrum and not its surface core-level shifted partner, we can clearly see that they are very similar. This indicates that the measured PED patterns must originate predominantly from the same Eu layer, the fifth subsurface Eu layer. This layer thus exhibits a noninteger valency. There are some small additional features, which can be seen in Fig. 3(d). They appear due to the overlap of the Eu $4f$ multiplet with PE from valence states. Their influence becomes particularly strong for the Eu-terminated surface because the PE signal from the bulk Eu^{2+} component has a much smaller intensity in comparison to its surface partner [see Fig. 2(c)]. The corresponding computed PED patterns, shown in Figs. 3(h) and 3(i), are almost identical and the very tiny differences between them are related to the different kinetic energies of $4f$ photoelectrons from Eu^{2+} and Eu^{3+}.

It should be noted that all the computed PED patterns in Fig. 3 agree well with the measured ones. This fact indicates that all our assumptions made above are reasonable for PED analysis of the considered system.

To determine the Eu valencies in different layers more precisely, we analyzed relative PE intensities of Eu^{2+} and

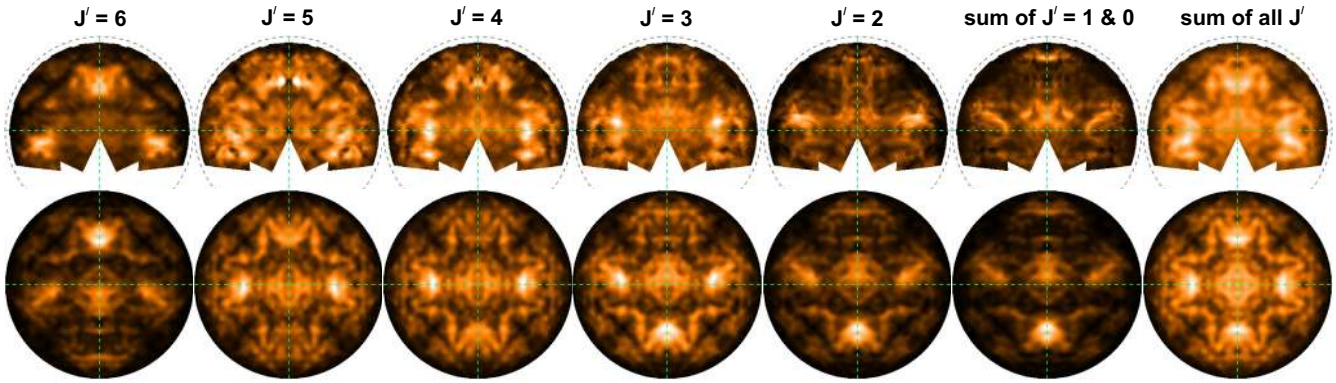

FIG. 4. Experimental (upper row) and computed (lower row) PED patterns of Eu^{2+} $4f$ multiplet of the magnetically ordered Eu layer below the Si-terminated surface at $T = 30$ K. The color scale is identical for both experimental and theoretical patterns with the same J'. Magnetization vector points to the left.

Eu^{3+} $4f$ multiplets. For this purpose, we have measured PE spectra for the two crystal terminations in the off-resonance conditions at the photon energies of 110, 160, and 200 eV. Then we calculated the intensities, taking into account PED, and determined which concentrations in different layers give good agreement with the measured data for all photon energies. The fact that the first Eu layer is fully divalent allows us to estimate the valency in the fifth layer from the intensity ratio of the bulk and surface Eu^{2+} components, which is about $1/10$ in Fig. 2(c). A similar estimation can be obtained from the ratio of Eu^{3+} and surface Eu^{2+} peak intensities. Supposing that the valency in the ninth Eu layer is close to the bulk value of 2.8, we obtained the valency of the fifth layer as 2.77 ± 0.07, where the uncertainty was estimated from the scatter of results obtained for different photon energies.

In the analysis of PE intensities for the Si-terminated surface, we assumed the Eu valency in the 12th layer to be 2.8 and took into account the ratio of Eu^{3+} concentrations in the fourth and eighth layers determined from the PED analysis. As a result, we obtained the valency of 2.1 ± 0.05 for the fourth layer and 2.4 ± 0.2 for the eighth layer. Thus, the valency of the eighth layer at the Si termination notably deviates from the bulk value in contrast to the fifth layer at the Eu termination, which already shows bulk properties.

So far, we considered only the integrated intensity of the whole Eu^{2+} multiplet. However, it is of great interest to also analyze the individual components with different J'. It represents a certain challenge, since the individual J' components of the Eu $4f$ multiplet are closely packed in a small energy window. However, they can be resolved in the PE spectrum for the Eu^{2+} multiplet obtained from the Si-terminated surface, as seen in Fig. 2(b). The experimental PED patterns are shown in the upper part of Fig. 4. Note that the components with $J' = 0$ and 1 cannot be well separated due to a small energy difference. Therefore, they were treated as a single feature. As expected, each component demonstrates its own PED pattern. Moreover, they do not exhibit the fourfold symmetry that is intrinsic for the studied crystal, and only the mirror plane is observed in each pattern.

These observations clearly indicate the presence of magnetization at the surface, which lowers the symmetry of the system as observed in the PED patterns. The only source of magnetism can be the fourth Eu layer, which behaves divalently. Therefore, to model the "magnetic" PED patterns, we used Eqs. (9) and (4). In the calculations, we neglect the contributions from the deeper Eu layers and consider only the signal from the fourth layer. The resulting angular distributions of the photocurrent strongly depend on the direction of magnetization through the D matrix in Eq. (7). Therefore, the direction of magnetization can be determined by comparison of calculated and measured PED patterns. From the previous studies, we already know that it is aligned in the surface plane along the [100] direction [14]. Hence, there are four possible orientations of magnetization. For the case of the studied sample, the computed PED patterns are shown in the lower row of Fig. 4. They exhibit good agreement with the experimental data when the magnetization is directed to the left relative to the measured patterns.

Reasonably good overall agreement indicates that the data were collected predominantly from a single magnetic domain, although we did not magnetize the sample before measurements. Moreover, it is possible to conclude that our model captures the most essential physical effects, which define the PE intensity maps. However, there are many fine features observed in the PED patterns that were not reproduced in the model calculations. The main reason for that is the presence of the fine dispersions of the $4f$ states due to their momentum-dependent hybridization with valence-band states [24]. In the respective avoided-crossing regions, reliable separation of the Eu $4f$ multiplet components is impossible. Moreover, our simple PE model is not expected to describe the intensity of hybridized states.

It is worth noting that the analysis of separate multiplet components in the Eu^{2+} signal from the noninteger-valent fifth Eu layer below the Eu-terminated surface did not reveal any asymmetry. This is consistent with our expectations that the fifth Eu layer is not magnetically ordered.

As we have seen, the wide-angle PED patterns give a lot of information about the properties of the crystal surface, but individual PE spectra can also be useful for the analysis of magnetic ordering in the near-surface layers. Let us consider them in more detail.

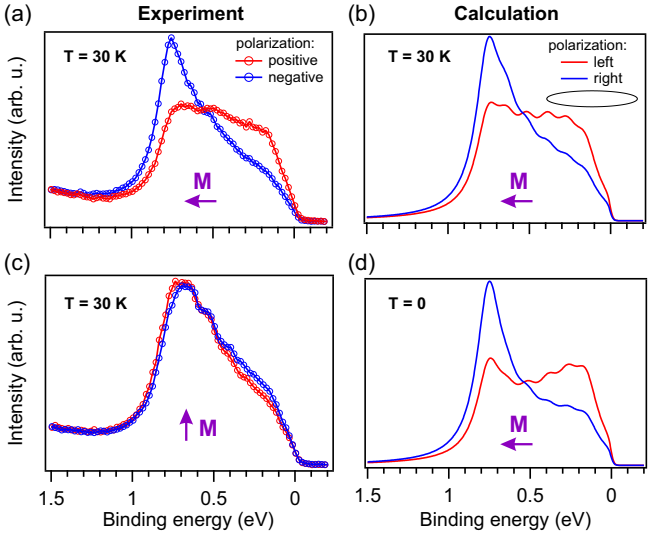

FIG. 5. (a), (c) Measured MCD in the PE of the Eu^{2+} multiplet of the Si-terminated surface. (b), (d) Calculated MCD spectra taking into account PED at the crystal surface. The ellipse illustrates the polarization of photons. The arrow shows the magnetization (**M**) direction relative to the horizontal measurement plane. Positive and negative polarizations correspond to the PEARL beamline settings, while left and right notations are used in the EDAC program.

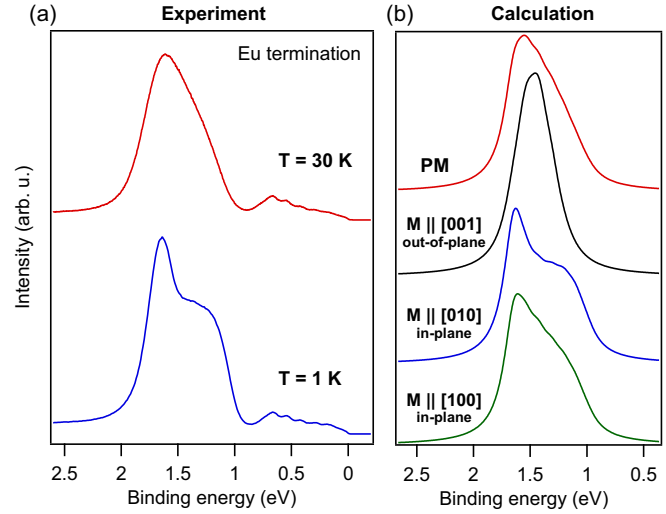

FIG. 6. (a) XPS spectra of the Eu^{2+} $4f$ multiplet for the Eu-terminated surface measured at different temperatures using linear polarization of photons. (b) Calculated Eu^{2+} spectra of the topmost Eu layer for PM and FM phases with different orientations of magnetization **M** at zero temperature.

D. Analysis of 4*f* spectral shape

All PED patterns discussed in this paper were measured with linear polarization of photons, however, elliptical or circular polarization is known to be useful for the studies of magnetic materials [33]. Further, we discuss a magnetic circular dichroism (MCD) experiment on $EuIr_2Si_2$, using the elliptical polarization of photons. Two spectra of the Eu^{2+} multiplet were measured with opposite elliptical polarizations for two different sample orientations. The spectra in Fig. 5(a) were taken in a geometry where the beam, the analyzer axis, the surface normal, and the magnetization vector were all in one plane. In this case, strong dichroism is observed, as expected for a magnetized material [34]. The $4f$ PE spectra in Fig. 5(c) were measured after rotation of the sample by 90° about the surface normal so magnetization became nearly orthogonal to this plane. Consequently, the MCD signal has almost fully disappeared. This observation is consistent with our statement that the PE spectra were acquired from a single magnetic domain.

To model the MCD spectra, we take into account PED, which may notably change the multiplet shape [35]. We set the polarization vector to $\vec{\varepsilon} = (\cos\alpha, \pm i\sin\alpha, 0)$ with $\alpha = 10^\circ$ and integrated the calculated PE intensity over the analyzer acceptance angle range, which was $\pm 20^\circ$. The multiplet components were modeled as Lorentzian functions with a half width of 90 meV and binding energies set to the experimentally determined values. The MCD spectra calculated for two different temperatures are shown in Figs. 5(b) and 5(d). They demonstrate sensitivity of the multiplet shape to the occupation of the ground-state M_J sublevels. Apparently, the spectrum calculated for the temperature of the experiment, $T = 30\,\mathrm{K}$, exhibits notably better agreement with the measured data than the spectrum for $T = 0$, indicating the importance of considering the temperature effects.

It should be noted that we did not observe any MCD effect in the Eu^{2+} PE spectra taken from the Eu-terminated surface at $T = 30\,\mathrm{K}$. Thus, it either remains in the PM phase or the Eu surface reveals a mosaic of small magnetic domains from which we obtain the averaged signal. However, these two possibilities can be easily discriminated by modeling the spectral shape of the Eu^{2+} $4f$ multiplet.

In Fig. 6(a), we show two spectra taken from the Eu-terminated surface at the temperatures of 30 K and 1 K. They exhibit strikingly different spectral shapes that is a clear indication that magnetic ordering is different for these two cases. Figure 6(b) demonstrates simulated $4f$ multiplets for the PM phase and for FM ordering with different orientations of the magnetization. Here, the [100] and [001] directions lie in one plane with the photon beam and the analyzer axis. The half width of the multiplet components was set to 110 meV. Although we took into account the PED, the diffraction effect does not play an important role here. This is because the PE intensity is integrated (along the [010] direction) over the wide acceptance angle of the spectrometer. Thus, the computed Eu^{2+} PE spectra are rather similar to those obtained experimentally from the crystalline Eu-terminated surface. The essential result of our calculations is a strong dependence of the spectral shape on the direction of magnetization (a magnetic linear dichroism). From the comparison of experimental and theoretical spectra, it is evident that the Eu-terminated surface shows no magnetic ordering at $T = 30\,\mathrm{K}$, while at $T = 1\,\mathrm{K}$ it becomes magnetic with in-plane orientation of the magnetic moments. Note that the shape of the subsurface (bulk) Eu^{2+} multiplet is rather similar for these two temperatures. This indicates that the fifth Eu layer is not magnetically ordered at 1 K, which is in agreement with the PED results implying that the mean valency of the Eu ions in the fifth Eu layer is close to the bulk value of 2.8.

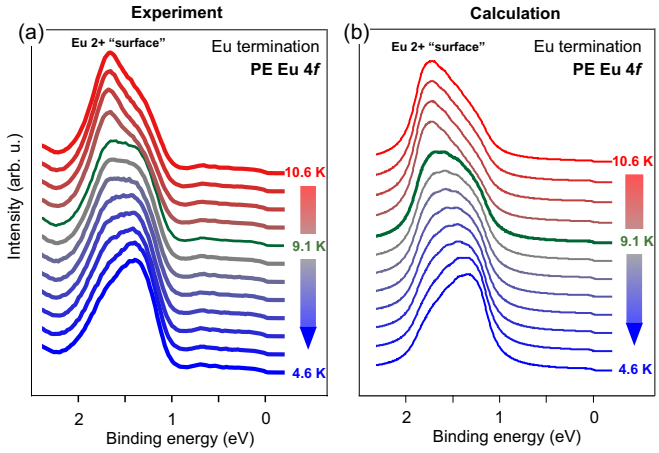

FIG. 7. (a) Measured and (b) computed [using Eq. (9)] normal-emission XPS spectra of the Eu^{2+} $4f$ multiplet for the Eu-terminated surface as a function of temperature at circular polarization of photons. The measurements were performed at the SIS beamline using a photon energy of 110 eV. The critical temperature in the calculation was set to 9.5 K and magnetization was oriented in the [100] direction.

To clarify the Curie temperature for the Eu termination, we measured the temperature dependence of the Eu $4f$ PE spectra using circularly polarized photons. Strongest changes of spectral shape are expected when the magnetization direction is along [100] (in the measurements plane). Therefore, it was important to find a correctly oriented magnetic domain on the sample surface. The experimental results are shown in Fig. 7(a). They demonstrate strong changes in the Eu $4f$ multiplet at the temperatures below $\sim$10 K. The measured spectra are in good agreement with the calculated PE spectra shown in Fig. 7(b), where the Curie temperature was set to $T_C = 9.5$ K. However, it is worth noting that the T_C value obtained from different sets of spectra was varying from about 11 K for the freshly cleaved sample to about 8 K after several hours of measurements. This fact implies that the T_C value is rather sensitive to surface contamination.

IV. CONCLUSIONS

In summary, we have developed a methodology allowing us to analyze the properties of layered $4f$ materials with focus on the magnetism and valency of rare-earth ions in the absence of CEF splitting of the ground state. The developed model was applied to study the surface-related properties of $EuIr_2Si_2$, which reveals temperature-dependent fluctuating valency in the bulk. We considered two possible surface terminations of this crystal that are Eu and Si surfaces and explored how the valency of Eu ions changes from the surface to deeper lying Eu layers. We also investigated the magnetic order of these Eu layers.

For the Si-terminated surface, we have found that Eu ions in the fourth atomic layer behave divalently, however, PED analysis reveals a small admixture of the trivalent state, resulting in a mean valence of 2.1 ± 0.05. Analysis of the PED patterns taken from individual components of the Eu $4f$ multiplet of Eu^{2+} ions have shown that they exhibit a ferromagnetic order below 48 K. The latter lowers the symmetry of the PED patterns and the emergent spontaneous magnetization lies within the surface plane along the [100] direction. Moreover, in presence of magnetization, the PED patterns taken for individual $^7F_{J'}$-multiplet components become notably different from each other, in contrast to the PM phase. The performed analysis shows that information about the orientation of the $4f$ magnetic moments can be derived from these PED patterns. The next deeper (eighth) Eu atomic layer below the Si-terminated surface contains Eu ions with a noninteger valency of 2.4 ± 0.2, which is lower than the valency in the bulk.

For the Eu-terminated surface, we determined the value of the surface relaxation, which was found to match the DFT prediction perfectly. Temperature-dependent studies revealed a ferromagnetic ordering in the first Eu layer with the Curie temperature of about 10 K and an in-plane orientation of the $4f$ moments. We found that the next (fifth) Eu layer is not magnetically ordered and reveals already a noninteger valency close to the value in the bulk. Thus, the fifth layer for the Eu termination is more bulklike than the deeper eighth layer for the Si termination.

Our results demonstrate that PED applied to a layered rare-earth intermetallic material with an open $4f$ shell provides valuable insight into the crystal-surface structure, chemical state of rare-earth atoms and their relation to the magnetic order with ultimate depth resolution. Besides successful description of angular distributions of photoelectrons produced with linearly polarized photons, our approach allowed us to accurately model the MCD in PE, taking into account the PED effects at the crystal surface. Finally, we have shown that the simple picture of direct PE may still be valid at the maximum of a giant resonance in the $4f$ PE cross section, allowing selective enhancement of sensitivity to lanthanide atoms. We assume that the presented approach may also be useful for investigations of other rare-earth-based materials, where similar or even more complex interlacing properties linked with magnetism in the surface region may be found, which might have been overlooked so far.

ACKNOWLEDGMENTS

This work was supported by the Russian Foundation for Basic Research (Grant No. 20-32-70127), the Ministry of Science and Higher Education of the Russian Federation [Grant No. 075-15-2020-797 (13.1902.21.0024)], Saint Petersburg State University (Grant No. ID 51126254), and the German Research Foundation (DFG) through Grants No. KR-3831/5-1, No. LA655/20-1, No. GRK1621, No. SFB1143 (Project No. 247310070), and ProjectNo. 422213477–TRR 288. D.V.V. acknowledges financial support from the Spanish Ministry of Economy (MAT-2017-88374-P). E.V.Ch. acknowledges the Tomsk State University competitiveness improvement program (Grant No. 8.1.01.2018). S.I.F. acknowledges Japan Society for the Promotion of Science (KAKENHI Grant No. JP16H01084). We thank the Paul Scherrer Institut, Villigen, Switzerland for provision of synchrotron radiation beamtime at beamlines PEARL and SIS of the SLS.

[1] C. S. Fadley, X-ray photoelectron spectroscopy: Progress and perspectives, J. Electron Spectrosc. Relat. Phenom. **178–179**, 2 (2010).

[2] C. Westphal, The study of the local atomic structure by means of x-ray photoelectron diffraction, Surf. Sci. Rep. **50**, 1 (2003).

[3] D. P. Woodruff, Surface structural information from photoelectron diffraction, J. Electron Spectrosc. Relat. Phenom. **178–179**, 186 (2010).

[4] F. Matsui, T. Matsushita, and H. Daimon, Holographic reconstruction of photoelectron diffraction and its circular dichroism for local structure probing, J. Phys. Soc. Jpn. **87**, 061004 (2018).

[5] M. V. Kuznetsov, I. I. Ogorodnikov, D. Yu. Usachov, C. Laubschat, D. V. Vyalikh, F. Matsui, and L. V. Yashina, Photoelectron diffraction and holography studies of 2D materials and interfaces, J. Phys. Soc. Jpn. **87**, 061005 (2018).

[6] A. Verdini, P. Krueger, and L. Floreano, in *Surface Science Techniques*, edited by G. Bracco and B. Holst, Vol. 51 (Springer-Verlag, Berlin, 2013), Chap. VIII, pp. 217.

[7] K. Tsutsui, T. Matsushita, K. Natori, T. Muro, Y. Morikawa, T. Hoshii, K. Kakushima, H. Wakabayashi, K. Hayashi, F. Matsui, and T. Kinoshita, Individual atomic imaging of multiple dopant sites in As-doped Si using spectro-photoelectron holography, Nano Lett. **17**, 7533 (2017).

[8] E. D. Tober, F. J. Palomares, R. X. Ynzunza, R. Denecke, J. Morais, Z. Wang, G. Bino, J. Liesegang, Z. Hussain, and C. S. Fadley, Observation of a Ferromagnetic-To-Paramagnetic Phase Transition on a Ferromagnetic Surface Using Spin-Polarized Photoelectron Diffraction: Gd(0001), Phys. Rev. Lett. **81**, 2360 (1998).

[9] T. Matsushita and F. Matsui, Features of atomic images reconstructed from photoelectron, Auger electron, and internal detector electron holography using SPEA-MEM, J. Electron Spectrosc. Relat. Phenom. **195**, 365 (2014).

[10] M. Treier, P. Ruffieux, R. Fasel, F. Nolting, S. Yang, L. Dunsch, and T. Greber, Looking inside an endohedral fullerene: Inter- and intramolecular ordering of $Dy_3N@C_{80}(I_h)$ on Cu(111), Phys. Rev. B **80**, 081403(R) (2009).

[11] P. Krüger, S. Bourgeois, B. Domenichini, H. Magnan, D. Chandesris, P. Le Fèvre, A. M. Flank, J. Jupille, L. Floreano, A. Cossaro, A. Verdini, and A. Morgante, Defect States at the TiO_2(110) Surface Probed by Resonant Photoelectron Diffraction, Phys. Rev. Lett. **100**, 055501 (2008).

[12] B. Chevalier, J. M. D. Coey, B. Lloret, and J. Etourneau, $EuIr_2Si_2$–A new intermediate mixed valence compound, J. Phys. C: Solid State Phys. **19**, 4521 (1986).

[13] U. Stockert, S. Seiro, N. Caroca-Canales, E. Hassinger, and C. Geibel, Valence effect on the thermopower of Eu systems, Phys. Rev. B **101**, 235106 (2020).

[14] S. Schulz, I. A. Nechaev, M. Güttler, G. Poelchen, A. Generalov, S. Danzenbächer, A. Chikina, S. Seiro, K. Kliemt, A. Y. Vyazovskaya, T. K. Kim, P. Dudin, E. V. Chulkov, C. Laubschat, E. E. Krasovskii, C. Geibel, C. Krellner, K. Kummer, and D. V. Vyalikh, Emerging 2D-ferromagnetism and strong spin-orbit coupling at the surface of valence-fluctuating $EuIr_2Si_2$, npj Quantum Mater. **4**, 26 (2019).

[15] S. Seiro and C. Geibel, From stable divalent to valence-fluctuating behavior in $Eu(Rh_{1-x}Ir_x)_2Si_2$ single crystals, J. Phys.: Condens. Matter. **23**, 375601 (2011).

[16] S. Seiro, Y. Prots, K. Kummer, H. Rosner, R. C. Gil, and C. Geibel, Charge, lattice and magnetism across the valence crossover in $EuIr_2Si_2$ single crystals, J. Phys.: Condens. Matter **31**, 305602 (2019).

[17] D. Yu. Usachov, M. Güttler, S. Schulz, G. Poelchen, S. Seiro, K. Kliemt, K. Kummer, C. Krellner, C. Laubschat, E. V. Chulkov, and D. V. Vyalikh, Spin structure of spin-orbit split surface states in a magnetic material revealed by spin-integrated photoemission, Phys. Rev. B **101**, 245140 (2020).

[18] K. Kummer, Y. Kucherenko, S. Danzenbächer, C. Krellner, C. Geibel, M. G. Holder, L. V. Bekenov, T. Muro, Y. Kato, T. Kinoshita, S. Huotari, L. Simonelli, S. L. Molodtsov, C. Laubschat, and D. V. Vyalikh, Intermediate valence in Yb compounds probed by $4f$ photoemission and resonant inelastic x-ray scattering, Phys. Rev. B **84**, 245114 (2011).

[19] M. Muntwiler, J. Zhang, R. Stania, F. Matsui, P. Oberta, U. Flechsig, L. Patthey, C. Quitmann, T. Glatzel, R. Widmer, E. Meyer, T. A. Jung, P. Aebi, R. Fasel, and T. Greber, Surface science at the PEARL beamline of the Swiss Light Source, J. Sync. Rad. **24**, 354 (2017).

[20] F. J. García de Abajo, M. A. Van Hove, and C. S. Fadley, Multiple scattering of electrons in solids and molecules: A cluster-model approach, Phys. Rev. B **63**, 075404 (2001).

[21] D. Yu. Usachov, A. V. Tarasov, K. A. Bokai, V. O. Shevelev, O. Yu. Vilkov, A. E. Petukhov, A. G. Rybkin, I. I. Ogorodnikov, M. V. Kuznetsov, M. Muntwiler, F. Matsui, L. V. Yashina, C. Laubschat, and D. V. Vyalikh, Site- and spin-dependent coupling at the highly ordered h-BN/Co(0001) interface, Phys. Rev. B **98**, 195438 (2018).

[22] C. Pan, S. L. Carter, and H. P. Kelly, Resonance structure due to the $4d^{10}4f^7 \rightarrow 4d^94f^8$ transition in the photoionization cross section of atomic europium, Phys. Rev. A **43**, 1290 (1991).

[23] G. Kaindl, A. Höhr, E. Weschke, S. Vandre, C. Schussler-Langeheine, and C. Laubschat, Surface core-level shifts and surface states for the heavy lanthanide metals, Phys. Rev. B **51**, 7920 (1995).

[24] S. Danzenbächer, D. V. Vyalikh, Y. Kucherenko, A. Kade, C. Laubschat, N. Caroca-Canales, C. Krellner, C. Geibel, A. V. Fedorov, D. S. Dessau, R. Follath, W. Eberhardt, and S. L. Molodtsov, Hybridization Phenomena in Nearly-Half-Filled f-Shell Electron Systems: Photoemission Study of $EuNi_2P_2$, Phys. Rev. Lett. **102**, 026403 (2009).

[25] D. V. Vyalikh, S. Danzenbächer, Y. Kucherenko, C. Krellner, C. Geibel, C. Laubschat, M. Shi, L. Patthey, R. Follath, and S. L. Molodtsov, Tuning the Hybridization at the Surface of a Heavy-Fermion System, Phys. Rev. Lett. **103**, 137601 (2009).

[26] M. G. Silly, F. Charra, F. Lux, G. Lemercier, and F. Sirotti, The electronic properties of mixed valence hydrated europium chloride thin film, Phys. Chem. Chem. Phys. **17**, 18403 (2015).

[27] S. R. Mishra, T. R. Cummins, G. D. Waddill, W. J. Gammon, G. van der Laan, K. W. Goodman, and J. G. Tobin, Nature of Resonant Photoemission in Gd, Phys. Rev. Lett. **81**, 1306 (1998).

[28] K. Starke, Z. Hu, F. Hubinger, E. Navas, G. Kaindl, and G. van der Laan, Magnetic circular dichroism in lanthanide 4d-4f giant resonant photoemission: Terbium, Eur. Phys. J. B **12**, 171 (1999).

[29] A. P. Cox, Fractional parentage methods for ionisation of open shells of d and f electrons, *Photoelectron Spectrometry. Structure and Bonding* (Springer, Berlin, 1975), pp. 59–81.

[30] D. Varshalovich, A. Moskalev, and V. Khersonskii, *Quantum Theory Of Angular Momemtum* (World Scientific Publishing, Singapore, 1988).

[31] M. Getzlaff, *Fundamentals of Magnetism* (Springer, Berlin, 2008).

[32] C. Laubschat, G. Kaindl, W.-D. Schneider, B. Reihl, and N. Mårtensson, Stability of $4f$ configurations in rare-earth-metal compounds, Phys. Rev. B **33**, 6675 (1986).

[33] K. Starke, *Magnetic Dichroism in Core-Level Photoemission* (Springer, Berlin, 2000).

[34] E. Arenholz, K. Starke, G. Kaindl, and P. J. Jensen, Interfacial Magnetism of Eu/Gd(0001) Studied by Magnetic Circular Dichroism in Photoemission, Phys. Rev. Lett. **80**, 2221 (1998).

[35] S. Gorovikov, S. Bode, K. Starke, and G. Kaindl, Angular dependence of magnetic dichroism in 4f-photoemission, J. Magn. Magn. Mater. **198-199**, 665 (1999).